Title

Structural Insights into Activation of the Retinal L-type Ca2+ Channel (Cav1.4) by Ca2+-binding Protein 4 (CaBP4)*

Journal

Journal of Biological Chemistry, 289(45)

ISSN

0021-9258

Authors

Park, Saebomi
Li, Congmin
Haeseleer, Françoise
et al.

Publication Date

2014-11-01

DOI

10.1074/jbc.m114.604439

Peer reviewed

THE JOURNAL OF BIOLOGICAL CHEMISTRY VOL. 289, NO. 45, pp. 31262–31273, November 7, 2014

Structural Insights into Activation of the Retinal L-type Ca^{2+} Channel (Cav1.4) by Ca^{2+}-binding Protein 4 (CaBP4)*

Received for publication, August 12, 2014, and in revised form, September 23, 2014 Published, JBC Papers in Press, September 25, 2014, DOI 10.1074/jbc.M114.604439

Saebomi Park‡, Congmin Li‡, Françoise Haeseleer§, Krzysztof Palczewski¶1, and James B. Ames‡2

From the ‡Department of Chemistry, University of California, Davis, California 95616, the §Department of Physiology and Biophysics, University of Washington, Seattle, Washington 98195, and the ¶Department of Pharmacology, Cleveland Center for Membrane and Structural Biology, School of Medicine, Case Western Reserve University, Cleveland, Ohio 44106-4965

Background: Cav1.4 is regulated by CaBP4, which is required for continuous release of neurotransmitter in retinal photoreceptor cells.
Results: CaBP4 contains two separate EF-hand lobes that bind Ca^{2+} and form a collapsed structure around the IQ motif in Cav1.4.
Conclusion: CaBP4 is suggested to activate Cav1.4 by disrupting an interaction between IQ and ICDI.
Significance: CaBP4 mutations associated with congenital stationary night blindness impair its binding to IQ.

CaBP4 modulates Ca^{2+}-dependent activity of L-type voltage-gated Ca^{2+} channels (Cav1.4) in retinal photoreceptor cells. Mg^{2+} binds to the first and third EF-hands (EF1 and EF3), and Ca^{2+} binds to EF1, EF3, and EF4 of CaBP4. Here we present NMR structures of CaBP4 in both Mg^{2+}-bound and Ca^{2+}-bound states and model the CaBP4 structural interaction with Cav1.4. CaBP4 contains an unstructured N-terminal region (residues 1–99) and four EF-hands in two separate lobes. The N-lobe consists of EF1 and EF2 in a closed conformation with either Mg^{2+} or Ca^{2+} bound at EF1. The C-lobe binds Ca^{2+} at EF3 and EF4 and exhibits a Ca^{2+}-induced closed-to-open transition like that of calmodulin. Exposed residues in Ca^{2+}-bound CaBP4 (Phe^{137}, Glu^{168}, Leu^{207}, Phe^{214}, Met^{251}, Phe^{264}, and Leu^{268}) make contacts with the IQ motif in Cav1.4, and the Cav1.4 mutant Y1595E strongly impairs binding to CaBP4. We conclude that CaBP4 forms a collapsed structure around the IQ motif in Cav1.4 that we suggest may promote channel activation by disrupting an interaction between IQ and the inhibitor of Ca^{2+}-dependent inactivation domain.

CaBP4[3] is a 35-kDa Ca^{2+}-binding protein expressed in retinal photoreceptor cells, localized primarily at the synaptic bulb (1, 2). CaBP4 controls the continuous release of the glutamate neurotransmitter in dark state photoreceptor cells (3), by regulating L-type calcium channels (Cav1.4) (1, 4). The C-terminal regulatory region of Cav1.4 binds to CaBP4 (4), which enables channel activation at high cytosolic Ca^{2+} levels and hyperpolarized voltages (1). A distinctive characteristic of Cav1.4 is the lack of Ca^{2+}-dependent inactivation (CDI), because calmodulin (CaM) does not bind to its C-terminal region (5). Instead, Cav1.4 contains a stretch of residues in the C-terminal tail called the inhibitor of Ca^{2+}-dependent inactivation (ICDI) that prevents binding of CaM to the IQ motif. In addition, CaBP4 binding to Cav1.4 can prevent Ca^{2+}-dependent inactivation even in the absence of ICDI (4, 6).

Ca^{2+}-dependent regulation of Cav1.4 mediated by CaBP4 is genetically linked to congenital stationary night blindness (1). Particular mutations in both the *CACNA1F* gene that encodes the α_1-subunit of an L-type Ca^{2+} channel (Cav1.4α) (7–10) and the *CABP4* gene (11, 12) were associated with this autosomal recessive retinopathy. These findings are further underscored by observations that mice lacking either CaBP4 or Cav1.4α display a CSNB2-like phenotype (1, 13, 14). The first two mutations identified in the *CABP4* gene were c.800_801delAG and c.370C→T. The first c.800_801delAG mutation causes a frameshift, p.Glu267fs, which extends the protein by 91 novel amino acids and deletes its C terminus (11). In both humans and mice, mutations in *CABP4* lead to defective signaling between rods and cones with bipolar cells, wherein cones appear to be more affected. Thus, the phenotype presents more as a cone-rod dystrophy with a color vision deficit than congenital stationary night blindness.

CaBP4 belongs to a family of neuronal Ca^{2+}-binding proteins (CaBP1–5 (15)) and contains four EF-hands like those found in CaM and CaBP1 (16) (Fig. 1). By analogy to CaM (17), the four EF-hands are grouped into two domains connected by a central linker that is four residues longer in CaBP4 than in CaM. In contrast to CaM, CaBP4 contains ~100 non-conserved amino acids upstream of the EF-hands in the N-terminal region. Another distinguishing property of CaBP4 is that the second EF-hand lacks critical residues required for high affinity Ca^{2+} binding (15, 18).

Despite extensive studies on CaBP4 (1, 4, 6, 19), little is known about its structure and interaction with Ca^{2+} channel targets. Here, we present NMR solution structures of both Mg^{2+}-bound and Ca^{2+}-bound conformational states of CaBP4

* This work was supported, in whole or in part, by National Institutes of Health Grants EY012347 and RR11973 (University of California Davis NMR Facility) (to J. B. A.) and EY020850 (to F. H.).
The atomic coordinates and structure factors (codes 2M28 and 2M29) have been deposited in the Protein Data Bank (http://wwpdb.org/).
[1] John H. Hord Professor of Pharmacology.
[2] To whom correspondence should be addressed: Dept. of Chemistry, One Shields Ave., University of California, Davis, CA 95616. Tel.: 530-752-6358; Fax: 530-752-8995; E-mail: jbames@ucdavis.edu.
[3] The abbreviations used are: CaBP4, calcium-binding protein 4; HSQC, heteronuclear single quantum coherence; ICDI, inhibitor of Ca^{2+}-dependent inactivation; RMSD, root mean square deviation; CaM, calmodulin; ITC, isothermal titration calorimetry.

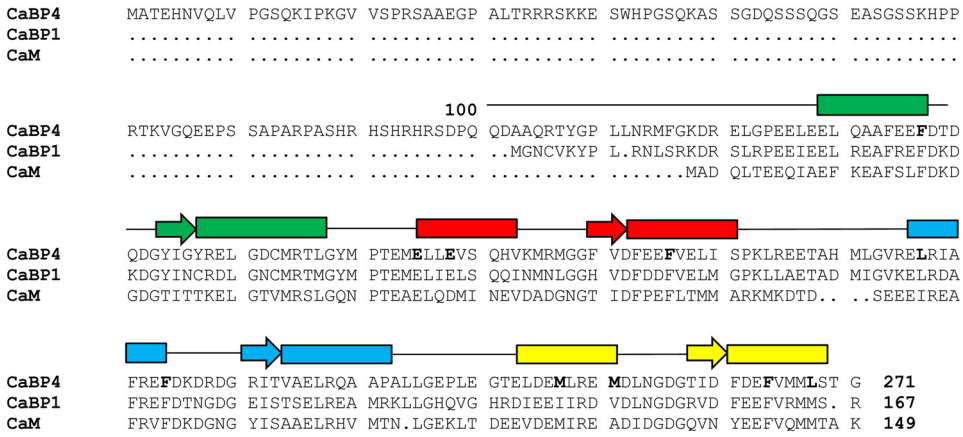

FIGURE 1. **Amino acid sequence alignment of mouse CaBP4, human CaBP1, and CaM.** Secondary structural elements (α-helices and β-strands) were derived from NMR analyses (21). The four EF-hands (EF1, EF2, EF3, and EF4) are *highlighted* in *green*, *red*, *cyan*, and *yellow*. Residues in CaBP4 that interact with the IQ motif are *highlighted* in *boldface type*.

and characterize the CaBP4 structural interaction with Cav1.4. CaBP4 NMR structures reveal important residues essential for its Ca^{2+}-dependent binding to Cav1.4. ITC and NMR analyses demonstrate that Ca^{2+}-saturated CaBP4 (but not the Ca^{2+}-free/Mg^{2+}-bound state) binds to the IQ motif in Cav1.4 (residues 1579–1605). All four EF-hands in CaBP4 contact the helical IQ motif and form a collapsed structure in the complex. Exposed residues in CaBP4 (Phe^{137}, Glu^{168}, Leu^{207}, Ile^{209}, Met^{251}, Phe^{264}, and Leu^{268}) make specific contacts with conserved residues in the IQ motif (Phe^{1586}, Ile^{1592}, Tyr^{1595}, and Arg^{1597}) that are essential for binding. We propose that CaBP4 activates Cav1.4 by binding to the IQ motif, which we suggest may disrupt an interaction between the IQ and ICDI domains.

EXPERIMENTAL PROCEDURES

Expression and Purification of CaBP4—Full-length mouse CaBP4 (residues 1–271) could not be concentrated beyond 1 mg/ml and therefore was not soluble enough for high resolution structural analysis by NMR. The first 99 residues from the N terminus of CaBP4 were shown to be unstructured, because this region was extensively cleaved in limited proteolysis studies (4). Removal of the first 99 residues of CaBP4 markedly improved protein solubility and did not affect target or Ca^{2+} binding. Thus, NMR experiments in this study were performed with the N-terminal deletion construct of CaBP4 (residues 100–271, called CaBP4(100–271)). Recombinant murine CaBP4(100–271) and mutants were subcloned into pET28 vector, expressed in Rosetta2(DE3) cells, and purified as described previously (20, 21).

CaBP4 N-lobe and C-lobe Fragments—cDNAs coding the CaBP4 N-terminal region (residues 1–100; called CaBP4(1–100)), CaBP4 N-lobe (residues 100–200; N-lobe), and CaBP4 C-lobe (residues 198–271; C-lobe) were cloned into protein expression vector pET28a. The recombinant proteins His_6-CaBP4(1–100), His_6-N-lobe, and His_6-C-lobe were expressed and purified by the same method used for CaBP4(100–271) (21).

Construction of CaBP4 Mutants—The M251A, F264E, and L268A mutants of CaBP4(100–271) were generated by using the QuikChange site-directed mutagenesis kit (Stratagene), and the mutations were confirmed by DNA sequencing. Mutant expression and purification procedures were the same as those used for wild type CaBP4.

Pull-down Assays with Cav1.4(1440–1982)—The mouse recombinant C-terminal regulatory region of Cav1.4 (residues 1440–1982, called Cav1.4(1440–1982)) and the Y1595E mutant containing a GST tag were cloned, expressed, and purified as noted before (22). GST pull-down assays were used to monitor binding of CaBP4 to Cav1.4(1440–1982)-GST as described previously (23). Protein samples of CaBP4 and Cav1.4(1440–1982)-GST were dissolved in Buffer A (0.1% Triton X-100, 150 mM NaCl, 10 mM $CaCl_2$, 10 mM Tris-HCl, pH 7.4, and protease inhibitors), concentrated to 0.5 ml (10 μM each), mixed with 0.5 ml of GST-Sepharose beads for 10 min, and then centrifuged for 5 min at 500 × *g*. Bead pellets were washed twice with Buffer A for 5 min at 4 °C. The samples were separated by SDS-PAGE, transferred for 10 h onto polyvinylidene fluoride (PVDF) membranes and probed with CaBP4 antibody.

NMR Spectroscopy—Samples for NMR analyses were prepared by dissolving unlabeled, ^{15}N-labeled, ^{15}N,^{13}C-labeled, or ^{2}H,^{13}C,^{15}N-labeled CaBP4 proteins (CaBP4(100–271, N-lobe, and C-lobe) in 0.3 ml of 90% H_2O, 10% [^{2}H]H_2O containing 10 mM [$^{2}H_{11}$]Tris, pH 7.4, 0.1 M KCl, and either 5 mM EDTA (apo), 5 mM $MgCl_2$ (Mg^{2+}-bound), or 5 mM $CaCl_2$ (Ca^{2+}-bound). All NMR experiments were performed at 37 °C on a Bruker Avance 800-MHz spectrometer equipped with a triple resonance cryoprobe and *z* axis gradient. Backbone and side chain NMR assignments for Ca^{2+}-bound CaBP4(100–271) and Mg^{2+}-bound N-lobe and C-lobe were determined as described previously (20, 21). All triple-resonance NMR experiments done for making resonance assignments were performed, processed, and analyzed as described (24) on a sample of ^{13}C/^{15}N-labeled Ca^{2+}-bound CaBP4(100–271) (or Mg^{2+}-bound N-lobe and C-lobe) with the following number of complex points and acquisition times: HNCO (^{15}N (F1) 32, 23.7 ms; ^{13}CO (F2) 64, 42.7 ms; ^{1}H (F3) 512, 64 ms); HNCACB (^{15}N (F1) 32, 23.7 ms; ^{13}C (F2) 48, 6.3 ms; ^{1}H (F3) 512, 64 ms); CBCACONNH (^{15}N (F1) 32, 23.7 ms; ^{13}C (F2) 48, 6.3 ms; ^{1}H (F3) 512, 64 ms); and HBHACONNH (^{15}N (F1) 32, 23.7 ms, $^{1}H_{ab}$ (F2) 64 21 ms, ^{1}H

TABLE 1
NMR structural statistics for Ca^{2+}-bound CaBP4

	Ca^{2+}-bound N-lobe	Ca^{2+}-bound C-lobe
Total NOE restraints	834	879
Intra	274	254
Medium	287	353
Long	135	140
Hydrogen bond restraints	54	40
Dihedral angle restraints	84	92
RMSD from ideal geometry		
Bond length (Å)	0.002 ± 0.001	0.0214 ± 0.001
Bond angle (degrees)	0.394 ± 0.026	1.122 ± 0.009
RMSD from average structure		
Backbone (Å)	0.53 ± 0.088	0.47 ± 0.092
Heavy atoms (degrees)	1.27 ± 0.102	1.10 ± 0.110
Ramachandran analysis (%)		
Most favored regions	82.0	74.2
Allowed regions	18.0	25.8
Disallowed regions	0.0	0.0

(F3) 512, 64 ms). ^{15}N-edited and ^{13}C-edited NOESY-HSQC (mixing time of 120 ms) and TOCSY-HSQC experiments were also performed as described previously (25). ^{1}H-^{15}N residual dipolar coupling constants (D_{NH}) were measured with a ^{15}N-labeled CaBP4 (~0.3 mM) containing 10 mg/ml Pf1 phage (Asla Biotech) and using a two-dimensional in phase/antiphase ^{1}H-^{15}N HSQC experiment (26). Heteronuclear {^{1}H}-^{15}N NOE experiments were performed using standard pulse sequences described previously (27). Steady-state {^{1}H}-^{15}N NOE values were obtained by recording two sets of spectra in the presence and absence of a 3-s proton saturation period. The NOE experiments were repeated three times to calculate the average and S.D. for the NOE values. All NMR data were processed and analyzed with the programs NMRPipe and nmrView.

NMR Structure Calculations—The structures were calculated with XPLOR-NIH (28), which employed the YASAP protocol (29). Distance restraints derived from interproton NOEs and dihedral angles (φ and ψ) from chemical shift index data are summarized in Table 1. Distance constraints were introduced for Ca^{2+} bound to loop residues 1, 3, and 5 in the EF1 closed state (30) and Ca^{2+} bound to loop residues 1, 3, 5, 7, and 12 in EF3 and EF4 (17). Fifty independent structures were calculated and refined using D_{NH} restraints as described (31). The final structural statistics are summarized in Table 1, and coordinates were deposited into the RCSB Protein Data bank (accession numbers 2M28 and 2M29).

Isothermal Titration Calorimetry—ITC experiments were performed using a VP-ITC calorimeter (MicroCal) at 30 °C, and data were acquired and processed with MicroCal software as described previously (32). Metal-free CaBP4 samples were prepared by exchanging CaBP4 protein into buffer containing 15 mM Tris-HCl, pH 7.5, 50 mM NaCl, and 1 mM tris(2-carboxyethyl)phosphine. The metal-free CaBP4(100–271) in the sample cell (120 μM, 1.5 ml) was titrated with either Ca^{2+} or Mg^{2+} (1 mM, 50 injections of 5 μl each).

CaBP4 binding to the Cav1.4 IQ motif was measured as described previously (18). CaBP4 was exchanged into buffer containing 15 mM Tris-HCl, pH 7.5, 500 mM NaCl, and 1 mM tris(2-carboxyethyl)phosphine with the addition of either 2 mM EDTA (apo-state), 5 mM $MgCl_2$ (Mg^{2+}-bound state) or 5 mM Ca^{2+} (Ca^{2+}-bound state). The IQ peptide (residues 1579–1605) at a concentration of 10 μM in the sample cell was titrated with CaBP4 (0.2 mM, delivered in 50 steps of 5 μl each). Data were analyzed with a one-site model using the MicroCal Origin 7 for ITC (33). The term "one-site model" refers to one type of site (having a particular K_d) with n number of these sites per protein molecule.

Docking Calculations—Separate structures for the Ca^{2+}-bound CaBP4 N-lobe and C-lobe were docked onto the helical structure of the IQ motif using HADDOCK (34–36). The helical structure of the Cav1.4 IQ motif was generated by SWISS-MODEL using the coordinates of the Cav1.2 IQ domain (Protein Data Bank code 2B6E) as a template. Docking was done with the Guru interface at the HADDOCK Web server (34–36). Mutagenesis data (IQ mutants: I1592A (4) and Y1595E, which weaken CaBP4 binding) and chemical shift perturbation data from ^{15}N-^{1}H HSQC (CaBP4 residues Leu^{122}, Leu^{130}, Phe^{137}, Leu^{157}, Phe^{186}, Leu^{207}, Phe^{214}, Leu^{235}, Met^{251}, Glu^{263}, Phe^{264}, and Leu^{268}) were used to define active and passive restraints (34). All together, 1000 rigid body docking runs, 200 structure calculation runs with torsion angle dynamics, and 200 refinements in explicit solvent were carried out. Resulting structures were clustered according to intermolecular energy terms and an RMSD from the lowest energy structure. The 15 lowest energy structures had an interface RMSD of 1.7 Å.

RESULTS

The N-terminal Region of CaBP4 Is Unstructured—Full-length CaBP4 (residues 1–271) tended to aggregate at protein concentrations needed for NMR (10 mg/ml) and was not soluble enough for structural analysis. The CaBP4 N-terminal region (residues 1–100) contains residues predicted to be unstructured (37). Indeed, the first 99 residues from the N terminus of CaBP4 were extensively cleaved in limited proteolysis studies (4), and an isolated 100-residue peptide fragment from CaBP4 (residues 1–100) is unstructured in solution based on having random coil NMR chemical shifts. Because the first 100 residues from the N terminus are unstructured, an N-terminal deletion construct was generated (residues 100–271 called CaBP4(100–271)) that is more soluble than full-length CaBP4 and adopts a well folded protein conformation in solution (21). The calorimetry and NMR structural studies described below were performed using CaBP4(100–271).

Ca^{2+} and Mg^{2+} Bind to CaBP4—Isothermal titration calorimetry (ITC) was used to analyze the energetics of Ca^{2+} and Mg^{2+} binding to CaBP4(100–271). Titration of Mg^{2+} into apo-CaBP4(100–271) produced an exothermic isotherm (Fig. 2*A*). Mg^{2+} is bound to CaBP4(100–271) with an apparent dissociation constant (K_d) of 83 μM, an enthalpy difference (ΔH) of −1.64 kcal/mol, and an n value of 2 (Table 2). The stoichiometry of Mg^{2+} binding was determined by analyzing ^{1}H-^{15}N HSQC NMR spectra of Mg^{2+}-bound CaBP4(100–271). NMR not only determines the number of ions bound per protein but can also determine which particular EF-hands are bound (32). Two downfield NMR peaks (diagnostic of Mg^{2+} binding (32)) indicate that two Mg^{2+} bind per protein. The two downfield peaks were assigned to Gly-143 (EF1) and Gly-220 (EF3), indicating that Mg^{2+} binds to CaBP4 at EF1 and EF3 (Fig. 2*A*, *inset*).

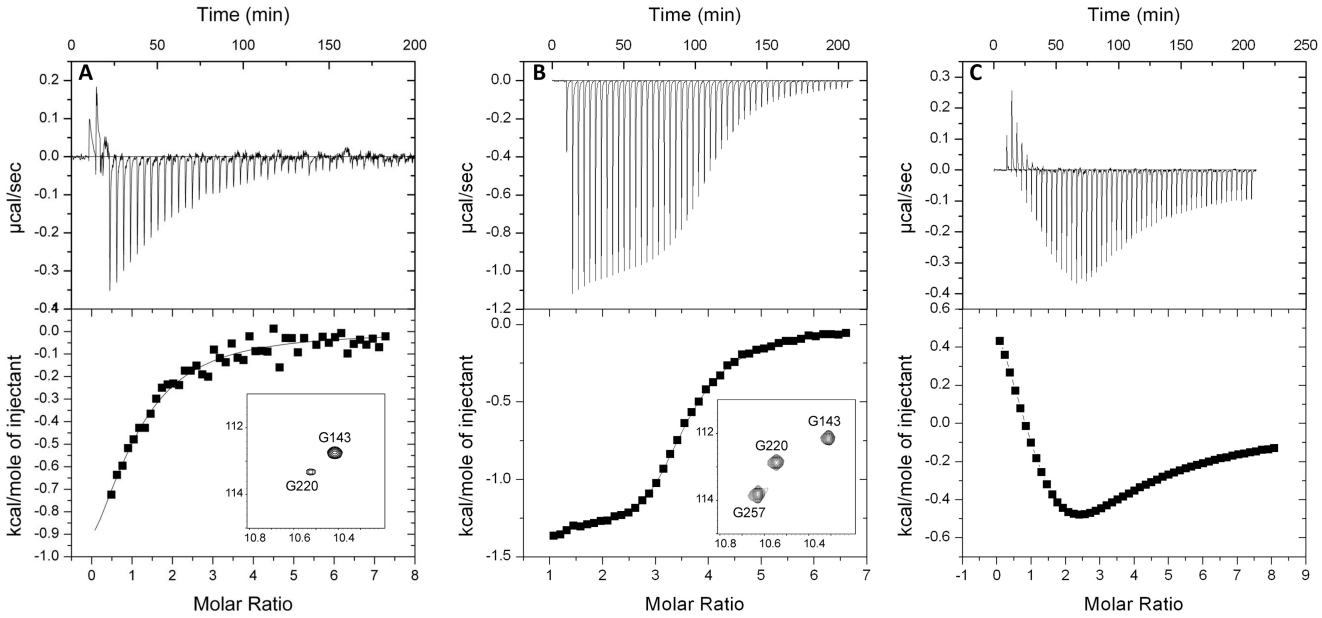

FIGURE 2. **CaBP4(100–271) binds to Mg^{2+} and Ca^{2+} as measured by ITC and NMR.** Binding isotherms are shown for Mg^{2+} binding (*A*), Ca^{2+} binding (*B*), and Ca^{2+} binding in the presence of 2 mM Mg^{2+} (*C*). Binding isotherms were fit to a one-site model, and fitting parameters are reported in Table 2. Downfield spectral regions of ^{1}H-^{15}N HSQC spectra of Mg^{2+} bound CaBP4(100–271) (*A*, *inset*) and Ca^{2+}-bound CaBP4(100–271) (*B*, *inset*) are also shown. The downfield peaks assigned to Gly^{143} and Gly^{220} (*A*, *inset*) indicate that Mg^{2+} is bound at EF1 and EF3, whereas peaks assigned to Gly^{143}, Gly^{220}, and Gly^{257} (*B*, *inset*) indicate that Ca^{2+} is bound at EF1, EF3, and EF4.

TABLE 2

ITC fitting parameters for CaBP4(100–271) binding to Mg^{2+}, Ca^{2+}, or IQ peptide at 30 °C

CaBP4(100–271) wild type is designated as $CaBP4^{WT}$, and CaBP4(100–271) mutants M251A, F264E, and L268A are designated as $CaBP4^{M251A}$, $CaBP4^{F264E}$, and $CaBP4^{L268A}$. CaBP4 C-lobe (residues 198–271) is designated as C-lobe.

Titration	K_d	ΔH^0	ΔS^0	*n*
	µM	*kcal mol*$^{-1}$	*cal mol*$^{-1}$ *K*$^{-1}$	
Mg^{2+} binding	83 ± 3	−1.6 ± 0.2	13 ± 1	2 ± 0.1
Ca^{2+} binding	6.0 ± 1	−1.4 ± 0.2	18 ± 1	3 ± 0.1
IQ binding to $CaBP4^{WT}$	0.8 ± 0.2	−2.5 ± 0.2	19 ± 1	0.9 ± 0.1
IQ binding to $CaBP4^{M251A}$	1.5 ± 0.3	−7.5 ± 0.5	1 ± 0.5	1 ± 0.1
IQ binding to $CaBP4^{F264E}$	2.5 ± 0.3	−2.9 ± 0.2	11 ± 1	1 ± 0.1
IQ binding to $CaBP4^{L268A}$	2.0 ± 0.3	−3.5 ± 0.5	14 ± 1	1 ± 0.1
IQ binding to C-lobe	20 ± 2	−1.4 ± 0.2	17 ± 1	1 ± 0.1

Titration of $CaCl_2$ into apo-CaBP4 (in the absence of Mg^{2+}) showed exothermic binding of three Ca^{2+} per protein (*n* value of 3) with an apparent K_d of 6 µM and a ΔH of −1.44 kcal/mol (Fig. 2*B* and Table 2). ^{1}H-^{15}N HSQC NMR spectra of Ca^{2+}-bound CaBP4(100–271) exhibited three downfield NMR peaks assigned to Gly-143 (EF1), Gly-220 (EF3), and Gly-257 (EF4), consistent with three Ca^{2+} bound per protein at EF1, EF3, and EF4 (Fig. 2*B*, *inset*).

To investigate whether Mg^{2+} competes with Ca^{2+} binding to CaBP4, the Ca^{2+}-binding isotherm was measured in the presence of physiological Mg^{2+} levels (2 mM) (Fig. 2*C*). The Ca^{2+}-binding isotherm in the presence of Mg^{2+} shows two separate phases: an initial endothermic binding at one site ($\Delta H = +0.5$ kcal/mol) followed by exothermic binding ($\Delta H = -1.9$ kcal/mol) at the other two sites. The endothermic Ca^{2+} binding to CaBP4(100–271) in the presence of Mg^{2+} contrasts with the overall exothermic binding of Ca^{2+} in the absence of Mg^{2+}. Also, the total enthalpy of Ca^{2+} binding became reduced in the presence of Mg^{2+}, consistent with endothermic dissociation of Mg^{2+} that precedes Ca^{2+} binding. The Mg^{2+} dependence of the Ca^{2+} binding isotherm suggests that Mg^{2+} competes with Ca^{2+} for binding to EF1 and EF3. In the photoreceptor cell, CaBP4 exists in the Ca^{2+}-bound state in the dark (high Ca^{2+}) and switches to the Mg^{2+}-bound state upon light activation when cytosolic Ca^{2+} levels decrease below 50 nM (38).

CaBP4 Has Two Independent Domains—CaM (39) and CaBP1 (32) both have four EF-hands divided into two structurally independent domains (an N-lobe and C-lobe) connected by a flexible linker. To test whether the EF-hands in CaBP4 form two independent domains, ^{1}H-^{15}N HSQC NMR spectra of an isolated lobe that contains EF1 and EF2 (N-lobe, residues 100–200) and a separate lobe that contains EF3 and EF4 (C-lobe, residues 198–271) were compared with spectra of full-length CaBP4 (Fig. 3, *A* and *B*). The backbone amide chemical shifts in the lobe fragments indicate that the individual lobes are stably folded. Also, the assigned chemical shifts in each lobe fragment were nearly identical to the corresponding chemical shifts of the full-length protein. Thus, the two isolated lobes are structurally independent, consistent with two non-interacting domains.

Heteronuclear ($\{^{1}H\}$-^{15}N) NOE analysis of CaBP4 reveals considerable backbone flexibility in the central linker that connects the two lobes (Fig. 3*C*). Relatively low heteronuclear NOE values (<0.6) were observed for residues 192–200 in the central linker region, indicating that CaBP4 does indeed contain a flexible interdomain linker. Heteronuclear NOE values (~0.8) are much higher for residues within each lobe and indicate that the two lobes are separately folded as shown previously for CaBP1 (32).

Structure of Ca^{2+}-bound CaBP4—The sequence-specific NMR assignments of CaBP4(100–271) were reported previously (21), and the secondary structure based on these assignments is summarized in Fig. 1. In the current study, we report the NMR structure of CaBP4(100–271) (Fig. 4). NMR-derived structures were calculated separately for the N-lobe (Protein

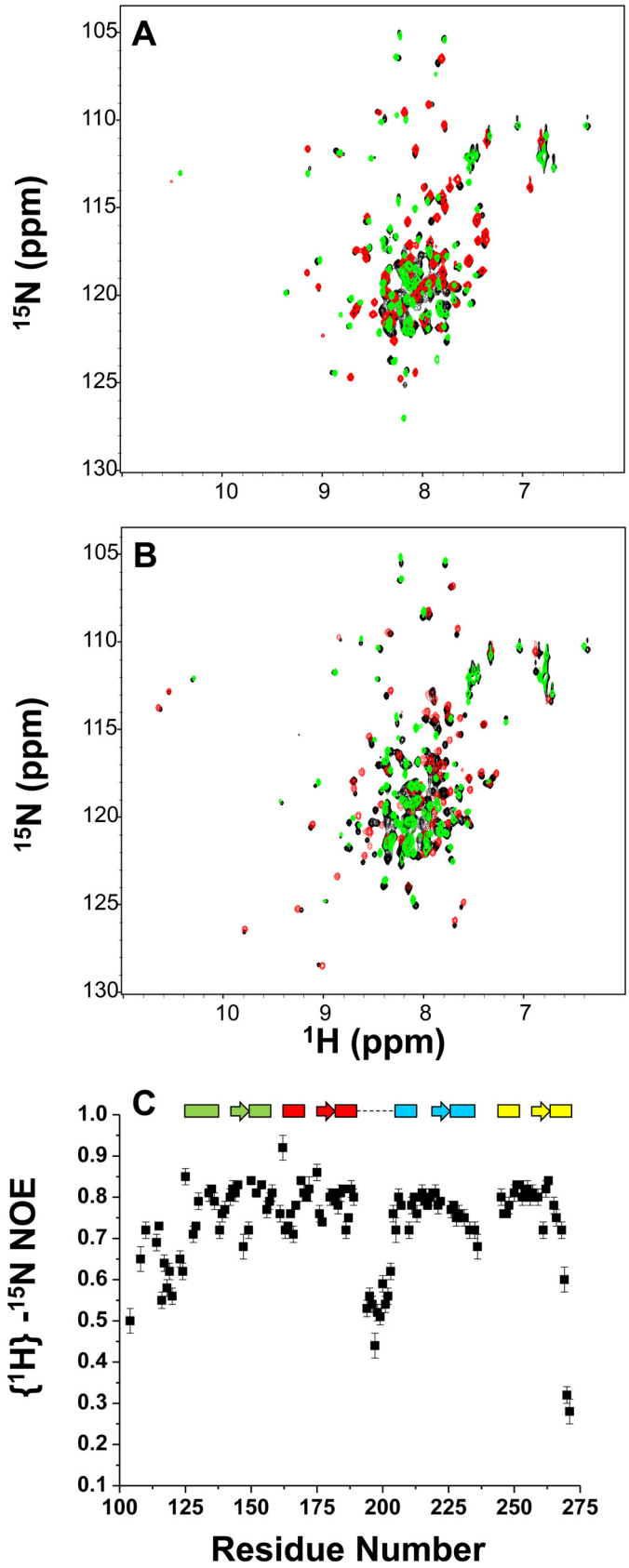

FIGURE 3. **CaBP4 has two independent domains.** Shown is an overlay of ^{1}H-^{15}N HSQC NMR spectra of CaBP4(100–271) (*black*), CaBP4 N-lobe (*red*), and C-lobe (*green*) in both Mg^{2+}-bound (*A*) and Ca^{2+}-bound (*B*) states. The spectral agreement of CaBP4(100–271) *versus* the individual lobes suggests that the N-lobe and C-lobe are both independently folded and non-interacting. *C*, {^{1}H}-^{15}N NOE data for Ca^{2+}-bound CaBP4 are plotted as a function of residue number. Secondary structure is shown schematically *above* the NOE data to illustrate that residues in the central linker region (*dotted line*) have low NOE values consistent with backbone flexibility.

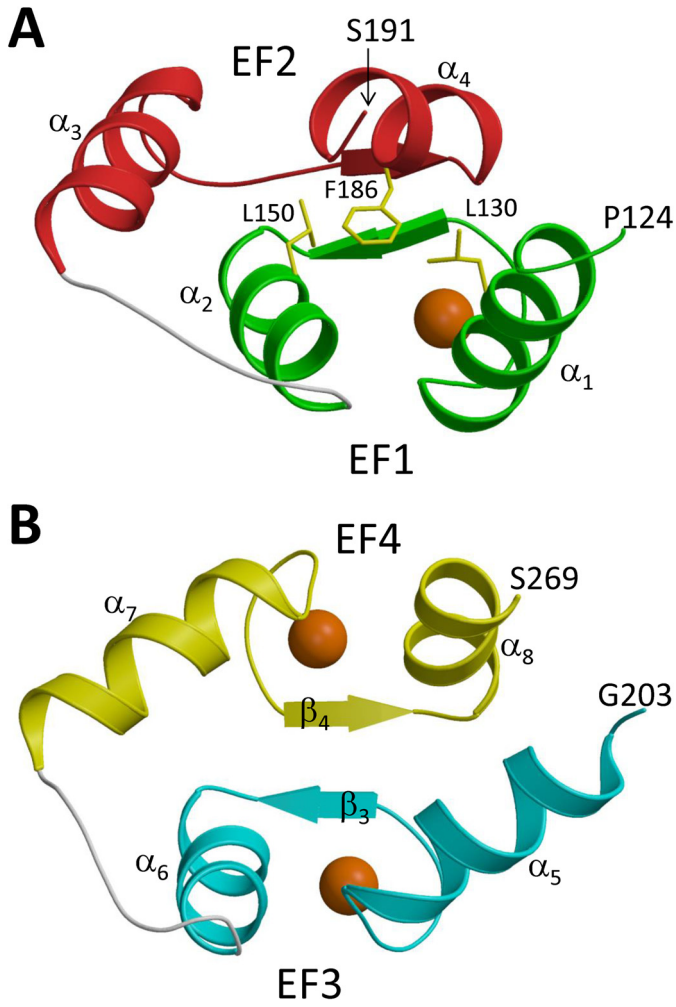

FIGURE 4. **NMR-derived structures calculated separately for the Ca^{2+}-bound CaBP4 N-lobe and C-lobe.** *Ribbon representations* of the energy-minimized average structure are illustrated for Ca^{2+}-bound N-lobe (Protein Data Bank code 2M29) (*A*) and Ca^{2+}-bound C-lobe (Protein Data Bank code 2M28) (*B*). The anti-parallel β-sheet has a horizontal orientation in both structures. N-terminal residues (residues 1–100) are unstructured and not shown. EF-hands are *highlighted* in *color* as defined in Fig. 1. *Orange spheres* represent bound Ca^{2+}. Hydrophobic side chain atoms of Leu^{130}, Leu^{150}, and Phe^{186} buried inside the closed N-lobe are *highlighted* in *yellow*.

Data Bank code 2M29) and C-lobe (Protein Data Bank code 2M28) using NOE-based distances and dihedral angle restraints that served as input for restrained molecular dynamics structure calculations (see "Experimental Procedures"). Statistics for the structure calculation are summarized in Table 1 for the 15 lowest energy conformers. The NMR-derived structures of CaBP4(100–271) were validated with PROCHECK: 82% of N-domain residues and 74.2% of C-domain residues belonged to the most favorable region on the Ramachandran plot.

The NMR-derived structure of Ca^{2+}-saturated CaBP4(100–271) (Fig. 4) contains a total of eight α-helices and four β-strands: α1 (residues 125–137), α2 (residues 147–156), α3 (residues 163–174), α4 (residues 183–190), α5 (residues 204–

216), α6 (residues 224–230), α7 (residues 241–150), α8 (residues 261–267), β1 (residues 144–146), β2 (residues 180–182), β3 (residues 221–223), and β4 (residues 258–260). CaBP4 contains two separate domains comprising four EF hands; EF1 (*green*, residues 120–156) and EF2 (*red*, residues 163–190) form the N-lobe, and EF3 (*cyan*, residues 200–230) and EF4 (*yellow*, residues 241–271) form the C-lobe. Some residues (residues 177 and 178) of the EF2 loop are ill defined due to a lack of NMR restraints. Residues between EF1 and EF2 (residues 157–162) and residues between EF3 and EF4 (residues 231–240) are structurally disordered, consistent with $\{^1H\}$-^{15}N heteronuclear NOE data (<0.6).

CaBP4(100–271) contains Ca^{2+} bound at EF1, EF3, and EF4 (*orange spheres* in Fig. 4) as evidenced by characteristic Ca^{2+}-dependent amide chemical shift changes assigned to Gly-143 in EF1, Gly-220 in EF3, and Gly-257 in EF4 (Fig. 2*B*, *inset*). The geometry of the coordinate covalent bonds formed between chelating amino acid residues in CaBP4 and the bound Ca^{2+} could not be observed directly in our NMR study. Instead, the stereochemical geometry and chelation of Ca^{2+} bound at EF3 and EF4 was modeled with structural constraints derived from the x-ray crystal structure of Ca^{2+}-bound CaM (17), which closely resembles the binding site geometry conserved in other EF-hand proteins (40). Structure calculations performed without the metal binding restraints produced an overall similar fold, and the metal binding restraints decrease the main chain RMSD by 25%.

The N-lobe of CaBP4 with one Ca^{2+} bound at EF1 (EF2 unoccupied) adopts a "closed" conformation (41); the interhelical angles of EF1 and EF2 are 134.7 and 141.1°, respectively. That EF1 and EF2 both remain in a closed conformation even when Ca^{2+} is bound at EF1 suggests that the binding energy of one Ca^{2+} at EF1 (EF2 unoccupied) does not suffice to drive a closed-to-open transition. This implies that the binding energy of two Ca^{2+} are needed to drive formation of the open state and could explain why two EF-hands are paired together to form a lobe (Fig. 4*A*). The Ca^{2+}-bound closed conformation for the N-lobe in CaBP4 is similar to that of CaBP1 (42) with an RMSD of 0.9 Å.

The Ca^{2+}-bound C-lobe of CaBP4 (two Ca^{2+} bound) forms the familiar "open" conformation seen for other Ca^{2+}-bound EF-hand proteins (16). For Ca^{2+}-bound CaBP4, the interhelical angles of EF3 and EF4 are 104.1 and 88.3° and quite different from the interhelical angles of EF1 and EF2 in the closed conformation (Fig. 4*B* and Table 3).

Exposed Hydrophobic Patch in CaBP4—A surface representation of Ca^{2+}-bound CaBP4 is illustrated in Fig. 5. The N-lobe surface contains many negatively charged residues (Glu^{121}, Glu^{125}, Glu^{129}, Glu^{136}, Glu^{163}, and Glu^{168}, *highlighted* in *red* in Fig. 5*A*). Only a few hydrophobic residues (Leu^{122}, Leu^{150}, and Met^{164}) and basic residues (Arg^{120}, Arg^{155}, and Arg^{174}) are exposed on the N-lobe surface. By contrast, the C-lobe of Ca^{2+}-bound CaBP4 has an extensive array of solvent-exposed hydrophobic residues (Leu^{207}, Phe^{214}, Ile^{222}, Leu^{235}, Leu^{239}, Met^{251}, Phe^{264}, and Leu^{268}, *highlighted* in *yellow* in Fig. 5*B*). This exposed hydrophobic patch on the C-lobe makes important contacts with the Cav1.4 IQ motif (see below). The hydrophobic patch is surrounded peripherally by charged residues (Arg^{205}, Glu^{206}, Glu^{213}, Arg^{218}, Glu^{237}, Glu^{240}, Glu^{243}, Glu^{246}, and Glu^{250}) *highlighted* in *red* and *blue* in Fig. 5*B*. Exposed negatively charged residues (Glu^{243}, Glu^{246}, Asp^{245}, Glu^{250}, and Asp^{262}) are clustered on the back side of the protein, opposite the hydrophobic patch.

Structure of Mg^{2+}-bound CaBP4—In light-activated photoreceptor cells, CaBP4 exists in a Mg^{2+}-bound state, because light activation decreases the cytosolic Ca^{2+} level below 50 nM

TABLE 3
Interhelical angles of the EF-hands in CaM and CaBP4

Helix pair	Interhelical angles			
	Apo-CaM[a]	Ca^{2+}-bound CaM[b]	Mg^{2+}-bound CaBP4[c]	Ca^{2+}-bound CaBP4[c]
	degrees			
EF1 (α_1-α_2)	130.9	103.8	133.8	134.7
EF2 (α_3-α_4)	130.8	101.0	140.7	141.1
EF3 (α_5-α_6)	139.5	101.0	140.1	104.1
EF4 (α_7-α_8)	126.0	101.0	128.2	88.3

[a] For apo-CaM (Protein Data Bank code 1DMO), residues in the helices are as follows: 6–18 (α1), 29–38 (α2), 45–55 (α3), 65–75 (α4), 82–90 (α5), 103–112 (α6), 118–127 (α7), and 137–143 (α8).
[b] For Ca^{2+}-bound CaM (Protein Data Bank code 1J7P), residues in the helices are as follows: 6–19 (α1), 29–38 (α2), 45–55 (α3), 65–75 (α4), 83–92 (α5), 102–111 (α6), 118–128 (α7), and 138–145 (α8).
[c] For CaBP4, residues in the helices are as follows: 129–137 (α_1), 147–157 (α_2), 163–173 (α_3), 183–190 (α_4), 204–214 (α_5), 224–233 (α_6), 242–251 (α_7), and 261–269 (α_8).

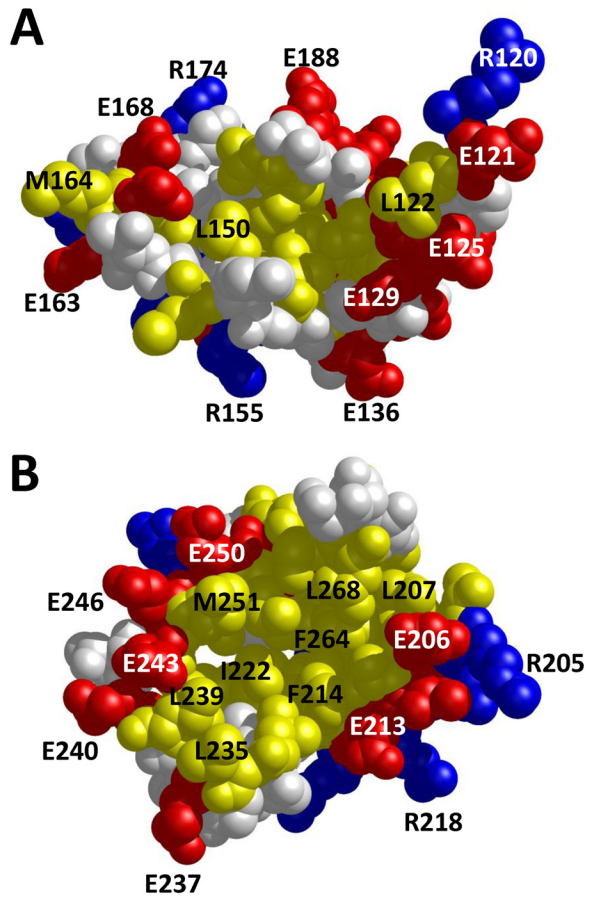

FIGURE 5. ***Space-filling representations* of Ca^{2+}-saturated CaBP4 illustrate exposed residues on the surface of the N-lobe (*A*) and C-lobe (*B*).** Acidic residues (Asp and Glu), basic residues (Arg, His, and Lys), and hydrophobic residues (Ile, Leu, Phe, Met, and Val) are *colored red*, *blue*, and *yellow*, respectively. C-lobe residues in the exposed hydrophobic patch make critical contacts with Cav1.4 (see below). The solvent-accessible hydrophobic surface area is 50 $Å^2$ for the N-lobe *versus* 92 $Å^2$ for the C-lobe.

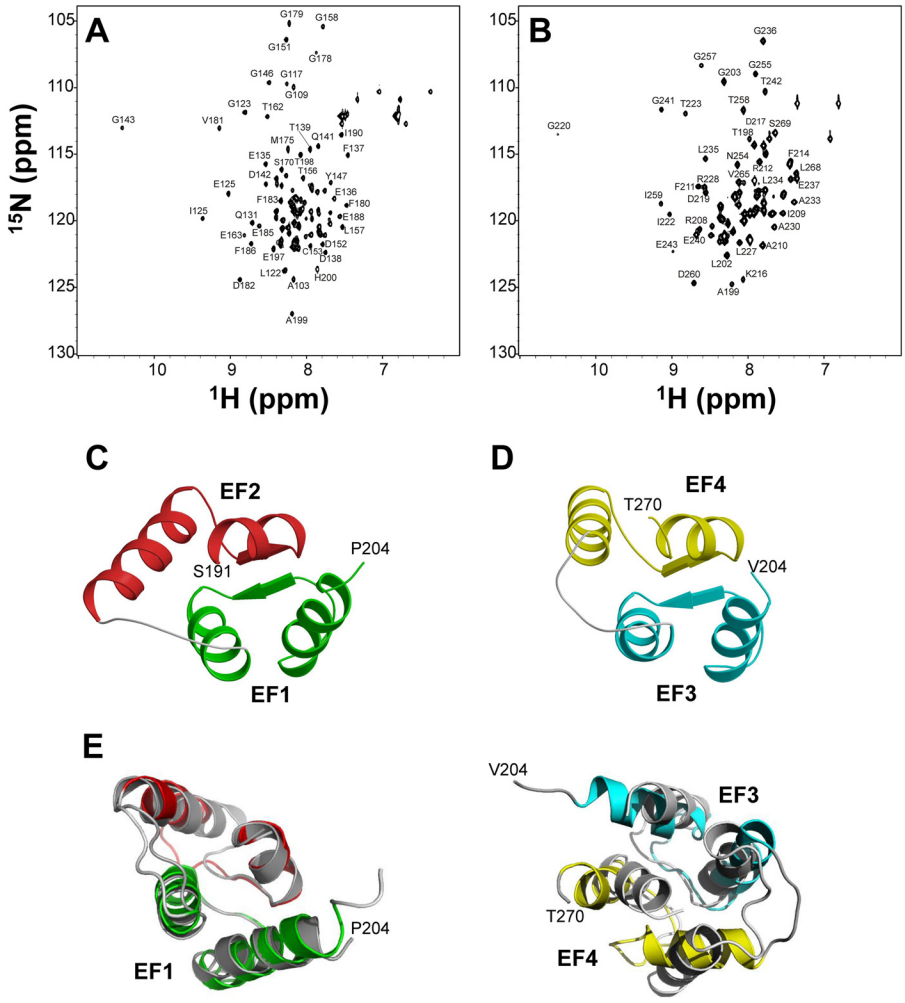

FIGURE 6. **NMR-based structures of Ca^{2+}-free/Mg^{2+}-bound CaBP4.** Shown are ^{1}H-^{15}N HSQC NMR spectra of Mg^{2+}-bound N-lobe (residues 100–200) (*A*) and Mg^{2+}-bound C-lobe (residues 198–271) (*B*). Resonance assignments are indicated by the residue labels. Downfield peaks at ~10.5 ppm are assigned to Gly^{143} (N-lobe) and Gly^{220} (C-lobe) and indicate that Mg^{2+} is bound at EF1 and EF3. Main chain structures of Ca^{2+}-free/Mg^{2+}-bound CaBP4 N-lobe (*C*) and C-lobe (*D*) were calculated using NMR residual dipolar couplings (31) and CS-ROSETTA (45). Bound Mg^{2+} ions at EF1 and EF3 are not shown. EF-hands are *highlighted* in *color* as defined in Fig. 1. *E*, structures of Ca^{2+}-free/Mg^{2+}-bound CaBP4 N-lobe (*left*) and C-lobe (*right*) *highlighted* in *gray* are overlaid onto structures of the Ca^{2+}-bound N-lobe (*left*) and C-lobe (*right*) shown in *color*. The N-lobe structure is not affected by Ca^{2+}, whereas the C-lobe exhibits a Ca^{2+}-induced decrease in interhelical angles for EF3 and EF4 (Table 3).

(38), whereas the physiological Mg^{2+} concentration remains steady at ~1 mM (43). Mg^{2+}-bound CaBP4(100–271) was not soluble enough for NMR structural analysis. Instead, NMR experiments were performed on separate constructs of the N-lobe (residues 100–200) and C-lobe (residues 198–271). ^{1}H-^{15}N HSQC spectra of Mg^{2+}-bound N-lobe and C-lobe fragments are shown in Fig. 6, *A* and *B*. These spectra contain downfield shifted peaks assigned to Gly-143 (EF1) and Gly-220 (EF3), indicating that Mg^{2+} is bound at EF1 and EF3, whereas EF2 and EF4 are unoccupied at saturating Mg^{2+} levels. Mg^{2+} binding at EF1 and EF3 was modeled based on the Mg^{2+}-bound structure of CaBP1 (32). Residues at the 1-, 3-, and 5-positions of the EF-hand loop (in EF1 and EF3) were selected to chelate the bound Mg^{2+} (30, 44). Separate protein structures of the Mg^{2+}-bound CaBP4 N-lobe and C-lobe were generated by CS-ROSETTA with HN, Cα, Cβ, and CO chemical shift values used as structural restraints (45). The five lowest energy structures were selected from 1000 trial structures and refined against the residual D_{NH} restraints as described (31). Initial residual dipolar coupling magnitude and rhombicity were calculated by fitting the measured residual dipolar couplings to the calculated structure using the PALES program (46). The residual dipolar coupling-refined structures of Mg^{2+}-bound N-lobe and C-lobe are presented in Fig. 6, *C* and *D*. The N-lobe structures have a quality *Q*-factor of 0.28 and an *R*-factor of 0.95, and the C-lobe structures have a *Q*-factor of 0.17 and an *R*-factor of 0.93. Both structures adopt a "closed" conformation in which the helices are nearly antiparallel with interhelical angles defined in Table 3. The overall secondary structure and topology of Mg^{2+}-bound CaBP1 are very similar to those described above for Ca^{2+}-bound CaBP4.

Ca^{2+}-induced Conformational Changes—Ca^{2+}-induced conformational changes in CaBP4 are illustrated by superimposing its Mg^{2+}-bound and Ca^{2+}-bound structures (Fig. 6*E*). For the CaBP4 N-lobe, the Ca^{2+}-bound closed conformation is similar to that of the Mg^{2+}-bound conformation (RMSD = 1.1 Å), indicating that Ca^{2+} binding to the N-lobe does *not* induce a significant conformational change. However, Ca^{2+} binding to the C-lobe at EF3 and EF4 caused large changes in the interhelical angles for both EF3 and EF4 (Table 3). This Ca^{2+}-induced

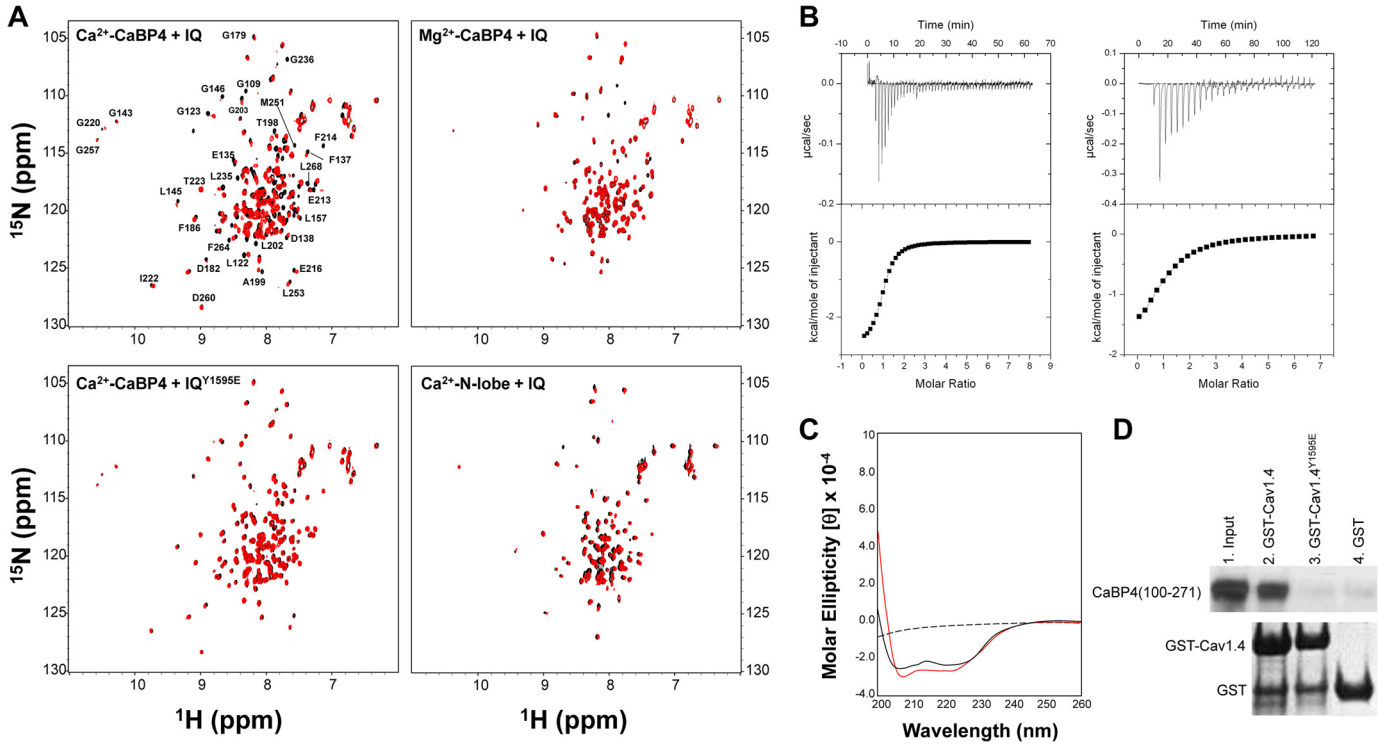

FIGURE 7. **CaBP4 binds to the Cav1.4 IQ motif (residues 1579–1605).** *A*, ^{1}H-^{15}N HSQC NMR spectra of Ca^{2+}-bound CaBP4(100–271) alone (*black*) and in the presence of the IQ peptide (*red*) (*top*, *left*); Mg^{2+}-bound CaBP4(100–271) alone (*black*) and in the presence of IQ peptide (*red*) (upper right); Ca^{2+}-bound CaBP4(100–271) alone (*black*) and in the presence of IQ peptide with Y1595E mutation (*red*) (*bottom*, *left*); and Ca^{2+}-bound N-lobe alone (*black*) and in the presence of IQ peptide (*red*) (*bottom*, *right*). The lack of IQ-induced spectral changes in the *bottom left panel* indicates a lack of CaBP4 binding to the Y1595E mutant peptide. *B*, ITC binding isotherm for Cav1.4 IQ peptide binding to Ca^{2+}-bound CaBP4(100–271) (*left*) and C-lobe (*right*). Experimental traces of the calorimetric titration (50 5-μl aliquots) are shown in the *top panels*, and the integrated binding isotherms are shown in the *bottom panels*. The steeper isotherm for CaBP4(100–271) binding to IQ compared with that of the C-lobe is consistent with its 10-fold higher affinity (Table 2), and both isotherms are consistent with a 1:1 binding stoichiometry. *C*, circular dichroism spectra of IQ alone (*black*, *dashed*), CaBP4(100–271) alone (*black*, *solid*), and CaBP4(100–271)-IQ complex (*red*). The CD spectrum of the IQ peptide free in solution (*dashed line*) indicates a random coil geometry. The CD spectrum of IQ bound to CaBP4 (*red*) reveals the emergence of positive ellipticity at 200 nm and enhanced negative ellipticity at 208 nm, consistent with the bound IQ forming an α-helix. *D*, representative GST pull-down assay (see "Experimental Procedures"). Recombinant CaBP4(100–271) (*input*, *lane 1*) was incubated with GST-Cav1.4(1440–1982) (*lane 2*), GST-Cav1.4(1440–1982) with the Y1595E mutation (*lane 3*), and GST alone (*lane 4*). Bound CaBP4(100–271) was detected by Western blotting with a specific antibody. The relative amount of each GST fusion protein used in the pull-down assay is indicated by the marked band intensities in the SDS-PAGE (*bottom*).

decrease in interhelical angles for both EF3 and EF4 is consistent with the familiar closed-to-open transition seen previously in CaM and other Ca^{2+} sensor proteins (16).

CaBP4 Binds to the IQ Motif in Cav1.4—CaBP4 was suggested previously to interact with the IQ motif (residues 1579–1605) in Cav1.4 (4). NMR and ITC experiments were performed to quantify CaBP4 binding to a peptide fragment that represents the IQ motif. NMR spectral changes in ^{15}N-^{1}H HSQC spectra of ^{15}N-labeled Ca^{2+}-bound CaBP4(100–271) were observed upon adding unlabeled IQ peptide (Fig. 7*A*). These spectral changes saturated after adding 1 eq of peptide, consistent with a 1:1 stochiometry. Injection of the IQ peptide into Ca^{2+}-bound CaBP4(100–271) showed exothermic binding ($\Delta H = -2.5$ kcal/mol) with 1:1 stoichiometry and a dissociation constant (K_d) of 0.8 μM (Fig. 7*B* (*left*) and Table 2). By contrast, the Ca^{2+}-free/Mg^{2+}-bound CaBP4 did not show any detectable binding to the IQ peptide as judged by a lack of NMR spectral changes in the ^{15}N-^{1}H HSQC spectra of CaBP4 after adding a 10-fold excess peptide (Fig. 7*A*, *top right*). ITC binding experiments showed that the IQ peptide binds to Ca^{2+}-bound CaBP4(100–271) with at least 10-fold higher affinity than it binds to the isolated C-lobe fragment (Fig. 7*B* (*right*) and Table 2). No ITC heat signals could be detected upon adding IQ peptide to the N-lobe, consistent with a lack of binding, and the Ca^{2+}-bound N-lobe did not show any detectable binding to the IQ peptide as judged by a lack of NMR spectral changes after adding a 10-fold excess of this peptide (Fig. 7*A*, *bottom right*). The much higher affinity binding of the IQ peptide to CaBP4(100–271) compared with the isolated lobes suggested that both lobes of Ca^{2+}-bound CaBP4 bind cooperatively to the IQ peptide in contrast to apo-CaM (47, 48), in which only the C-lobe forms contacts with the IQ motif.

Structural Model of CaBP4 Bound to the IQ Motif—The relatively low solubility of the CaBP4-IQ complex has thus far hampered all efforts to directly solve the complex structure by NMR or x-ray crystallography. Instead, an experimentally guided computational approach was used to dock the NMR structures of Ca^{2+}-bound CaBP4 (Fig. 4) onto a modeled helical structure of the Cav1.4 IQ motif, derived from the helical Cav1.2 IQ motif seen in previous crystal structures (49, 50). The helical structure of the IQ peptide bound to CaBP4 was confirmed by circular dichroism (Fig. 7*C*). The docking calculation performed with HADDOCK (34–36) was experimentally constrained with chemical shift perturbation data obtained by comparing NMR spectra of CaBP4 alone and in the presence of IQ peptide (Fig. 7*A*). The NMR resonances of CaBP4 that

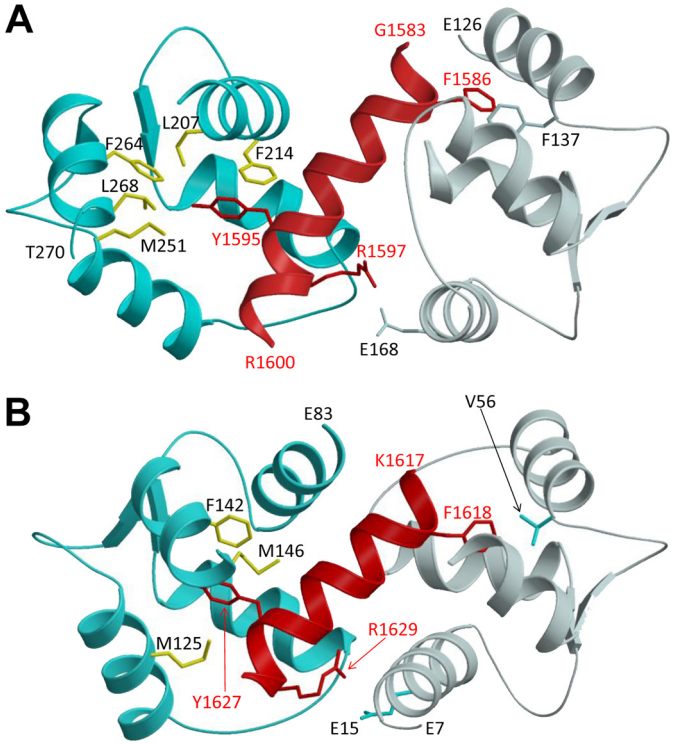

FIGURE 8. **Structural comparison of Ca^{2+}-bound CaBP4 and Ca^{2+}-bound CaM bound to the IQ motif.** *A*, structural model of the docked complex for CaBP4 (C-lobe (*cyan*) and N-lobe (*light gray*)) bound to Cav1.4 IQ motif (*red*). The docking calculation was performed using HADDOCK as described under "Experimental Procedures." *B*, structure of Ca^{2+}-bound CaM (C-lobe (*cyan*) and N-lobe (*light gray*)) bound to Cav1.2 IQ motif (*red*) from (49). Side chain atoms in the exposed hydrophobic patch of CaBP4 and CaM are *highlighted* in *yellow*.

showed largest changes in chemical shift were assigned to exposed residues (Glu^{121}, Leu^{122}, Gly^{123}, Phe^{137}, Met^{154}, Phe^{186}, Thr^{198}, Ala^{199}, Leu^{207}, Phe^{214}, Leu^{235}, Gly^{236}, Met^{251}, Glu^{263}, Phe^{264}, and Leu^{268}). Residues that affected this binding (see "Experimental Procedures") were selected as "active restraints" within HADDOCK to calculate an ensemble of docked structures (interface RMSD is 1.7 Å). A representative docked structure of CaBP4 bound to the IQ motif is shown in Fig. 8*A*.

Both lobes of Ca^{2+}-bound CaBP4 formed separate contacts with Cav1.4 on opposite sides of the IQ helix (C-lobe (*cyan*) and N-lobe (*light gray*) in Fig. 8*A*). Exposed hydrophobic residues in the CaBP4 C-lobe (Leu^{207}, Phe^{214}, Met^{251}, Phe^{264}, Leu^{268}) interacted primarily with Ile^{1592} and Tyr^{1595} on the same face of the IQ helix. This is consistent with the I1592A/Y1595A mutation in Cav1.4 that significantly weakened CaBP4 binding (4). In the current study, the Cav1.4 mutation, Y1595E, nearly abolished binding of CaBP4 to Cav1.4 in pull-down assays (Fig. 7*D*). Also, ^{15}N-^{1}H HSQC spectra of Ca^{2+}-bound CaBP4 remained unaffected by the addition of the Y1595E IQ mutant in contrast to large spectral changes caused by wild type IQ (Fig. 7*A*). Furthermore, mutating CaBP4 residues Met^{251}, Phe^{264}, and Leu^{268} that contact Tyr^{1595} (Fig. 8*A*) also weakened the binding to the IQ peptide. The CaBP4 mutants M251A, F264E, and L268A showed at least 2-fold weaker binding with a significant loss in binding entropy, consistent with the removal of a hydrophobic interaction for each mutant (Table 2). The CaBP4 C-lobe bound to the Cav1.4 IQ helix had the same relative orientation as the CaM C-lobe bound to the Cav1.2 IQ helix (49, 50) (Fig. 8*B*). The RMSD between main chain atoms of CaBP4 C-lobe *versus* CaM C-lobe in both complexes was 1.5 Å, suggesting that their overall main chain structures are fairly similar.

The CaBP4 N-lobe formed hydrophobic contacts and a salt bridge with the opposite face of the IQ helix (Fig. 8*A*). CaBP4 residue, Phe^{137} contacted Phe^{1586} on the IQ helix. The IQ residue, Arg^{1597} formed electrostatic contacts with CaBP4 residue, Glu^{168}. The IQ helix bound to the CaBP4 N-lobe had an opposite orientation compared with the Cav1.2 IQ helix bound to the CaM N-lobe (49, 50) (Fig. 8*B*). We suggest that the opposite orientation for the IQ helix bound to the CaBP4 N-lobe *versus* the CaM N-lobe might explain why L-type channels bind more tightly to CaBP4 than CaM (6).

We show that CaBP4 binds to the Cav1.4 IQ motif with a collapsed structure of both lobes that appears similar to the collapsed structure of Ca^{2+}-CaM bound to the Cav1.2 IQ (49, 50) (Fig. 8*B*). This similarity is consistent with the suggestion that CaBP4 binding to Cav1.4 can block CaM binding to prevent Ca^{2+}-dependent inactivation (5) and allow Cav1.4 channels to remain open at high Ca^{2+} levels in dark-adapted photoreceptor cells.

DISCUSSION

In this study, we determined the NMR solution structures of CaBP4 in both Mg^{2+}-bound and Ca^{2+}-bound conformational states and characterized the CaBP4 structural interaction with Cav1.4. The overall main chain structures of Mg^{2+}-bound and Ca^{2+}-bound CaBP4 (Figs. 4 and 6) are similar to those seen previously for CaBP1 (32). In the presence of physiological Mg^{2+} levels (and in the absence of Ca^{2+}), CaBP4 has Mg^{2+} bound at EF1 and EF3 (Fig. 2*A*, *inset*). At saturating Ca^{2+} levels, the N-lobe of CaBP4 adopts a closed conformation with Ca^{2+} bound at EF1 (and no metal bound at EF2), in contrast to the Ca^{2+}-bound open conformation seen in CaM (17) and TnC (51). The CaBP4 C-lobe binds Ca^{2+} at EF3 and EF4 (Fig. 2*B*, *inset*) and adopts the familiar Ca^{2+}-bound open conformation (Fig. 4*B*) with an exposed hydrophobic patch (Fig. 5). Many of the exposed hydrophobic residues in CaBP4 (Leu^{207}, Phe^{214}, Met^{251}, Phe^{264}, and Leu^{268}) make contact with the IQ motif (Fig. 8*A*). The corresponding residues in CaM make similar contacts with IQ, and this may explain why CaBPs and CaM compete for binding to IQ motifs in voltage-gated Ca^{2+} channels (52).

The Ca^{2+}-bound closed conformation for the CaBP4 N-lobe with Ca^{2+}-bound at EF1 (EF2 unoccupied; Fig. 4*A*) could prevent unwanted binding of low affinity molecules and play a role in enhancing target specificity in photoreceptors. The closed conformation of the Ca^{2+}-bound CaBP4 N-lobe conceals hydrophic residues (Leu^{130}, Leu^{150}, and Phe^{186} in Fig. 4*A*) that would otherwise be exposed in an open conformation. When CaBP4 binds to Cav1.4, we suggest that the target binding free energy may drive the closed Ca^{2+}-bound N-lobe into a semi-open conformation that can more readily recognize the IQ helix (53). Indeed, the modeled structure of CaBP4 bound to IQ peptide shows that the N-lobe (with Ca^{2+} bound at EF1) adopts a more opened conformation that exposes Phe^{137} and Phe^{186} to

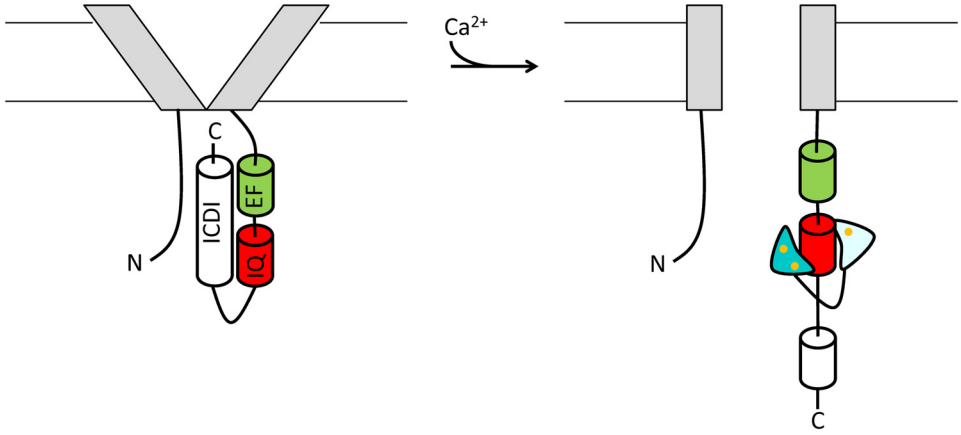

FIGURE 9. **Schematic model of Ca^{2+}-dependent channel opening for Cav1.4 mediated by CaBP4.** The Cav1.4 channel is shown in the closed state (*gray V-shaped box*) at low Ca^{2+} levels that exist in light-activated photoreceptors (*left*). Ca^{2+}-bound CaBP4 (C-lobe (*cyan*) and N-lobe (*light gray*)) binds to the IQ motif (*red*) at high cytosolic Ca^{2+} levels, which causes the Cav1.4 channel to remain in the open state (*gray parallel rectangles*) in dark-adapted photoreceptors (*right*). The ICDI domain (residues 1885–1984), IQ motif (residues 1579–1605), and EF-hand region (residues 1445–1493) are depicted by *white*, *red*, and *green cylinders*. *Orange circles* represent Ca^{2+} bound to CaBP4. The ICDI was suggested to interact with both the EF-hand region (5) and IQ (4, 6).

interact with Cav1.4 residue Phe^{1586} (Fig. 8*A*). This target-induced opening of the N-lobe (which lacks Ca^{2+}-binding at EF2) suggests that the target binding free energy can compensate for the lack of Ca^{2+} binding at EF2. Thus, disabling Ca^{2+} binding at EF2 in CaBP4 helps to ensure that the N-lobe remains closed in the absence of Cav1.4 to prevent binding of lower affinity molecules. A similar enhancement of target specificity is also seen for CaBP1 (42) and cardiac TnC (54), both of which have only one Ca^{2+} bound to the N-lobe.

The Cav1.4 IQ motif (residues 1579–1605) binds tightly to Ca^{2+}-bound CaBP4 but not to Ca^{2+}-free/Mg^{2+}-bound CaBP4. Ca^{2+}-dependent CaBP4 binding to IQ differs from the Ca^{2+}-independent binding of IQ motifs to CaM (47, 48) and other EF-hand proteins (55). The Cav1.4 IQ peptide binds to full-length CaBP4 with at least 10-fold higher affinity than IQ binding to the individual lobes. This positive cooperativity between the two lobes in CaBP4 is consistent with the collapsed structure of the two lobes that surround the IQ helix (Fig. 8). Similar cooperative lobe interactions are also seen in the crystal structures of Ca^{2+}-bound CaM bound to the Cav1.2 IQ (49, 50) and other protein targets (56).

CaBP4 makes primarily hydrophobic contacts with the IQ motif (Phe^{1586}, Tyr^{1587}, Ile^{1592}, and Tyr^{1595}). CaBP4 interacts most extensively with the Cav1.4 residue Tyr^{1595}, which we show is essential for binding (Fig. 7, *A* and *D*). CaBP4 residues (Leu^{207}, Met^{251}, and Leu^{268}) that contact Tyr^{1595} (Fig. 8*A*) are not conserved in CaM. These non-conserved hydrophobic contacts in the CaBP4-Cav1.4 complex could help explain why L-type channels bind more tightly to CaBP4 than to CaM (6).

Modulation of Cav1.4 by CaBP4 has been shown to be physiologically relevant by studies on knock-out mice and patients with retinal disease (1, 14). CaBP4 knock-out mice show defects in photoreceptor synaptic function and organization similar to those in mice that lack Cav1.4. In addition, homozygous mutations in both CaBP4 and Cav1.4 are associated with congenital stationary night blindness 2 (11, 57). In patients with pArg216X mutations, most of the CaBP4 C-lobe is absent, and this mutant form of CaBP4 cannot activate Cav1.4 (57). This is consistent with our finding that the CaBP4 N-lobe alone does not bind to the IQ motif (Fig. 7*A*). Patients with the c.800_801delAG deletion (lacking CaBP4 residues Glu^{263}–Gly^{271}) show an impaired modulation of Cav1.4 by CaBP4, leading to deficient neurotransmitter release from photoreceptors (11). This effect of deleting the C-terminal residues (Glu^{263}–Gly^{271}) is consistent with our structural model that indicates that Phe^{264} and Leu^{268} are important for contacting the IQ motif (Fig. 8*A*).

Based on our structure of the CaBP4-IQ complex (Fig. 8), we propose a schematic mechanism for Ca^{2+}-dependent regulation of Cav1.4 channel activity in photoreceptor cells (Fig. 9). In dark-adapted rods, the cytosolic Ca^{2+} concentration is maintained at high levels (38), which allows Ca^{2+}-bound CaBP4 to bind the IQ motif in Cav1.4. We suggest that CaBP4 binding to IQ could prevent IQ association with ICDI. The Cav1.4 IQ motif was suggested to interact with ICDI and promote channel closure, because deletion of the ICDI causes channel opening (4). The ICDI was also suggested to interact with the EF-hand region (residues 1445–1493, *highlighted* in *green* in Fig. 9*A*) (5). We suggest that Ca^{2+}-induced CaBP4 binding to IQ could disrupt the ICDI domain from interacting with both the IQ and EF-hand region and thus destabilize the Cav1.4 closed state at high Ca^{2+} levels. Therefore, Ca^{2+}-induced binding of CaBP4 to IQ is proposed to stabilize the Cav1.4 open state at high Ca^{2+} levels so that the channels remain open in dark-adapted photoreceptors. Light activation of these photoreceptors produces a drop in cytosolic Ca^{2+} (38) that in turn causes the Ca^{2+}-free CaBP4 to dissociate from Cav1.4. We propose that light-induced dissociation of Ca^{2+}-free CaBP4 would allow the IQ motif to interact with ICDI and promote channel closure upon light activation.

REFERENCES

1. Haeseleer, F., Imanishi, Y., Maeda, T., Possin, D. E., Maeda, A., Lee, A., Rieke, F., and Palczewski, K. (2004) Essential role of Ca^{2+}-binding protein 4, a Cav1.4 channel regulator, in photoreceptor synaptic function. *Nat. Neurosci.* **7,** 1079–1087
2. Maeda, T., Lem, J., Palczewski, K., and Haeseleer, F. (2005) A critical role of CaBP4 in the cone synapse. *Invest. Ophthalmol. Vis. Sci.* **46,** 4320–4327
3. Schmitz, F., Natarajan, S., Venkatesan, J. K., Wahl, S., Schwarz, K., and Grabner, C. P. (2012) EF hand-mediated Ca- and cGMP-signaling in pho-

toreceptor synaptic terminals. *Front. Mol. Neurosci.* **5,** 26
4. Shaltiel, L., Paparizos, C., Fenske, S., Hassan, S., Gruner, C., Rötzer, K., Biel, M., and Wahl-Schott, C. A. (2012) Complex regulation of voltage-dependent activation and inactivation properties of retinal voltage-gated Cav1.4 L-type Ca^{2+} channels by Ca^{2+}-binding protein 4 (CaBP4). *J. Biol. Chem.* **287,** 36312–36321
5. Wahl-Schott, C., Baumann, L., Cuny, H., Eckert, C., Griessmeier, K., and Biel, M. (2006) Switching off calcium-dependent inactivation in L-type calcium channels by an autoinhibitory domain. *Proc. Natl. Acad. Sci. U.S.A.* **103,** 15657–15662
6. Yang, P. S., Johny, M. B., and Yue, D. T. (2014) Allostery in Ca^{2+} channel modulation by calcium-binding proteins. *Nat. Chem. Biol.* **10,** 231–238
7. Hoda, J. C., Zaghetto, F., Singh, A., Koschak, A., and Striessnig, J. (2006) Effects of congenital stationary night blindness type 2 mutations R508Q and L1364H on Cav1.4 L-type Ca^{2+} channel function and expression. *J. Neurochem.* **96,** 1648–1658
8. Regus-Leidig, H., Atorf, J., Feigenspan, A., Kremers, J., Maw, M. A., and Brandstätter, J. H. (2014) Photoreceptor degeneration in two mouse models for congenital stationary night blindness type 2. *PLoS One* **9,** e86769
9. Strom, T. M., Nyakatura, G., Apfelstedt-Sylla, E., Hellebrand, H., Lorenz, B., Weber, B. H., Wutz, K., Gutwillinger, N., Rüther, K., Drescher, B., Sauer, C., Zrenner, E., Meitinger, T., Rosenthal, A., and Meindl, A. (1998) An L-type calcium-channel gene mutated in incomplete X-linked congenital stationary night blindness. *Nat. Genet.* **19,** 260–263
10. Wutz, K., Sauer, C., Zrenner, E., Lorenz, B., Alitalo, T., Broghammer, M., Hergersberg, M., de la Chapelle, A., Weber, B. H., Wissinger, B., Meindl, A., and Pusch, C. M. (2002) Thirty distinct CACNA1F mutations in 33 families with incomplete type of XLCSNB and Cacna1f expression profiling in mouse retina. *Eur. J. Hum. Genet.* **10,** 449–456
11. Zeitz, C., Kloeckener-Gruissem, B., Forster, U., Kohl, S., Magyar, I., Wissinger, B., Mátyás, G., Borruat, F. X., Schorderet, D. F., Zrenner, E., Munier, F. L., and Berger, W. (2006) Mutations in CABP4, the gene encoding the Ca^{2+}-binding protein 4, cause autosomal recessive night blindness. *Am. J. Hum. Genet.* **79,** 657–667
12. Bijveld, M. M., Florijn, R. J., Bergen, A. A., van den Born, L. I., Kamermans, M., Prick, L., Riemslag, F. C., van Schooneveld, M. J., Kappers, A. M., and van Genderen, M. M. (2013) Genotype and phenotype of 101 Dutch patients with congenital stationary night blindness. *Ophthalmology* **120,** 2072–2081
13. Lodha, N., Bonfield, S., Orton, N. C., Doering, C. J., McRory, J. E., Mema, S. C., Rehak, R., Sauvé, Y., Tobias, R., Stell, W. K., and Bech-Hansen, N. T. (2010) Congenital stationary night blindness in mice: a tale of two Cacna1f mutants. *Adv. Exp. Med. Biol.* **664,** 549–558
14. Mansergh, F., Orton, N. C., Vessey, J. P., Lalonde, M. R., Stell, W. K., Tremblay, F., Barnes, S., Rancourt, D. E., and Bech-Hansen, N. T. (2005) Mutation of the calcium channel gene Cacna1f disrupts calcium signaling, synaptic transmission and cellular organization in mouse retina. *Hum. Mol. Genet.* **14,** 3035–3046
15. Haeseleer, F., Sokal, I., Verlinde, C. L., Erdjument-Bromage, H., Tempst, P., Pronin, A. N., Benovic, J. L., Fariss, R. N., and Palczewski, K. (2000) Five members of a novel Ca^{2+}-binding protein (CABP) subfamily with similarity to calmodulin. *J. Biol. Chem.* **275,** 1247–1260
16. Ikura, M. (1996) Calcium binding and conformational response in EF-hand proteins. *Trends Biochem. Sci.* **21,** 14–17
17. Babu, Y. S., Bugg, C. E., and Cook, W. J. (1988) Structure of calmodulin refined at 2.2 Å resolution. *J. Mol. Biol.* **204,** 191–204
18. Wingard, J. N., Chan, J., Bosanac, I., Haeseleer, F., Palczewski, K., Ikura, M., and Ames, J. B. (2005) Structural analysis of Mg^{2+} and Ca^{2+} binding to CaBP1, a neuron-specific regulator of calcium channels. *J. Biol. Chem.* **280,** 37461–37470
19. Haeseleer, F., Sokal, I., Gregory, F. D., and Lee, A. (2013) Protein phosphatase 2A dephosphorylates CaBP4 and regulates CaBP4 function. *Invest. Ophthalmol. Vis. Sci.* **54,** 1214–1226
20. Park, S., Li, C., and Ames, J. (2010) ^{1}H, ^{15}N, and ^{13}C chemical shift assignments of calcium-binding protein 1 with Ca^{2+} bound at EF1, EF3 and EF4. *Biomol. NMR Assign.* **4,** 159–161
21. Park, S., Li, C., and Ames, J. (2014) ^{1}H, ^{15}N, and ^{13}C chemical shift assignments of murine calcium-binding protein 4. *Biomol. NMR Assign.* **8,** 361–364
22. Sun, W., Feng, R., Hu, H., Guo, F., Gao, Q., Shao, D., Yin, D., Wang, H., Sun, X., Zhao, M., Minobe, E., Sun, Y., Jiao, G., Kameyama, M., and Hao, L. (2014) The Ca^{2+}-dependent interaction of calpastatin domain L with the C-terminal tail of the Cav1.2 channel. *FEBS Lett.* **588,** 665–671
23. Minobe, E., Asmara, H., Saud, Z. A., and Kameyama, M. (2011) Calpastatin domain L is a partial agonist of the calmodulin-binding site for channel activation in Cav1.2 Ca^{2+} channels. *J. Biol. Chem.* **286,** 39013–39022
24. Clore, G. M., and Gronenborn, A. M. (1998) Determining the structures of large proteins and protein complexes by NMR. *Curr. Opin. Chem. Biol.* **2,** 564–570
25. Muhandiram, D. R., Farrow, N. A., Xu, G., Smallcombe, S. H., and Kay, L. E. (1993) A gradient NOESY-HSQC experiment for recording NOESY spectra of proteins dissolved in H_2O. *J. Magn. Reson. B* **102,** 317–321
26. Ottiger, M., Delaglio, F., and Bax, A. (1998) Measurement of J and dipolar couplings from simplified two-dimensional NMR spectra. *J. Magn. Reson.* **131,** 373–378
27. Farrow, N. A., Muhandiram, R., Singer, A. U., Pascal, S. M., Kay, C. M., Gish, G., Shoelson, S. E., Pawson, T., Forman-Kay, J. D., and Kay, L. E. (1994) Backbone dynamics of a free and phosphopeptide-complexed Src homology 2 domain studied by ^{15}N NMR relaxation. *Biochemistry* **33,** 5984–6003
28. Schwieters, C. D., Kuszewski, J. J., Tjandra, N., and Clore, G. M. (2003) The Xplor-NIH NMR molecular structure determination package. *J. Magn. Reson.* **160,** 65–73
29. Badger, J., Kumar, R. A., Yip, P., and Szalma, S. (1999) New features and enhancements in the X-PLOR computer program. *Proteins* **35,** 25–33
30. Senguen, F. T., and Grabarek, Z. (2012) X-ray structures of magnesium and manganese complexes with the N-terminal domain of calmodulin: insights into the mechanism and specificity of metal ion binding to an EF-hand. *Biochemistry* **51,** 6182–6194
31. Tjandra, N., and Bax, A. (1997) Direct measurement of distances and angles in biomolecules by NMR in a dilute liquid crystalline medium. *Science* **278,** 1111–1114
32. Li, C., Chan, J., Haeseleer, F., Mikoshiba, K., Palczewski, K., Ikura, M., and Ames, J. B. (2009) Structural insights into Ca^{2+}-dependent regulation of inositol 1,4,5-trisphosphate receptors by CaBP1. *J. Biol. Chem.* **284,** 2472–2481
33. Wiseman, T., Williston, S., Brandts, J. F., and Lin, L. N. (1989) Rapid measurement of binding constants and heats of binding using a new titration calorimeter. *Anal. Biochem.* **179,** 131–137
34. de Vries, S. J., van Dijk, M., and Bonvin, A. M. (2010) The HADDOCK web server for data-driven biomolecular docking. *Nat. Protoc.* **5,** 883–897
35. Dominguez, C., Boelens, R., and Bonvin, A. M. (2003) HADDOCK: a protein-protein docking approach based on biochemical or biophysical information. *J. Am. Chem. Soc.* **125,** 1731–1737
36. Tomaselli, S., Ragona, L., Zetta, L., Assfalg, M., Ferranti, P., Longhi, R., Bonvin, A. M., and Molinari, H. (2007) NMR-based modeling and binding studies of a ternary complex between chicken liver bile acid binding protein and bile acids. *Proteins* **69,** 177–191
37. Uversky, V. N., Radivojac, P., Iakoucheva, L. M., Obradovic, Z., and Dunker, A. K. (2007) Prediction of intrinsic disorder and its use in functional proteomics. *Methods Mol. Biol.* **408,** 69–92
38. Woodruff, M. L., Sampath, A. P., Matthews, H. R., Krasnoperova, N. V., Lem, J., and Fain, G. L. (2002) Measurement of cytoplasmic calcium concentration in the rods of wild-type and transducin knock-out mice. *J. Physiol.* **542,** 843–854
39. Chang, S. L., Szabo, A., and Tjandra, N. (2003) Temperature dependence of domain motions of calmodulin probed by NMR relaxation at multiple fields. *J. Am. Chem. Soc.* **125,** 11379–11384
40. Moncrief, N. D., Kretsinger, R. H., and Goodman, M. (1990) Evolution of EF-hand calcium-modulated proteins. *J. Mol. Evol.* **30,** 522–562
41. Yap, K. L., Ames, J. B., Swindells, M. B., and Ikura, M. (1999) Diversity of conformational states and changes within the EF-hand protein superfamily. *Proteins* **37,** 499–507
42. Park, S., Li, C., and Ames, J. B. (2011) Nuclear magnetic resonance structure of calcium binding protein 1 in a Ca^{2+}-bound closed state: implications for target recognition. *Protein Sci.* **20,** 1356–1366

43. Chen, C., Nakatani, K., and Koutalos, Y. (2003) Free magnesium concentration in salamander photoreceptor outer segments. *J. Physiol.* **553,** 125–135
44. Finley, N. L., Howarth, J. W., and Rosevear, P. R. (2004) Structure of the Mg^{2+}-loaded C-lobe of cardiac troponin C bound to the N-domain of cardiac troponin I: comparison with the Ca^{2+}-loaded structure. *Biochemistry* **43,** 11371–11379
45. Lange, O. F., Rossi, P., Sgourakis, N. G., Song, Y., Lee, H. W., Aramini, J. M., Ertekin, A., Xiao, R., Acton, T. B., Montelione, G. T., and Baker, D. (2012) Determination of solution structures of proteins up to 40 kDa using CS-Rosetta with sparse NMR data from deuterated samples. *Proc. Natl. Acad. Sci. U.S.A.* **109,** 10873–10878
46. Zweckstetter, M. (2008) NMR: prediction of molecular alignment from structure using the PALES software. *Nat. Protoc.* **3,** 679–690
47. Feldkamp, M. D., Yu, L., and Shea, M. A. (2011) Structural and energetic determinants of apo calmodulin binding to the IQ motif of the $Na_V1.2$ voltage-dependent sodium channel. *Structure* **19,** 733–747
48. Chagot, B., and Chazin, W. (2011) Solution NMR structure of Apo-calmodulin in complex with the IQ motif of human cardiac sodium channel NaV1. *J. Mol. Biol.* **406,** 106–119
49. Van Petegem, F., Chatelain, F. C., and Minor, D. L., Jr. (2005) Insights into voltage-gated calcium channel regulation from the structure of the CaV1.2 IQ domain-Ca^{2+}/calmodulin complex. *Nat. Struct. Mol. Biol.* **12,** 1108–1115
50. Fallon, J. L., Baker, M. R., Xiong, L., Loy, R. E., Yang, G., Dirksen, R. T., Hamilton, S. L., and Quiocho, F. A. (2009) Crystal structure of dimeric cardiac L-type calcium channel regulatory domains bridged by Ca^{2+} calmodulins. *Proc. Natl. Acad. Sci. U.S.A.* **106,** 5135–5140
51. Herzberg, O., and James, M. N. (1988) Refined crystal structure of troponin C from turkey skeletal muscle at 2.0 Å resolution. *J. Mol. Biol.* **203,** 761–779
52. Findeisen, F., Rumpf, C. H., and Minor, D. L., Jr. (2013) Apo states of calmodulin and CaBP1 control CaV1 voltage-gated calcium channel function through direct competition for the IQ domain. *J. Mol. Biol.* **425,** 3217–3234
53. Swindells, M. B., and Ikura, M. (1996) Pre-formation of the semi-open conformation by the apo-calmodulin C-terminal domain and implications binding IQ-motifs. *Nat. Struct. Biol.* **3,** 501–504
54. Li, M. X., Spyracopoulos, L., and Sykes, B. D. (1999) Binding of cardiac troponin-I147–163 induces a structural opening in human cardiac troponin-C. *Biochemistry* **38,** 8289–8298
55. Atkinson, R. A., Joseph, C., Kelly, G., Muskett, F. W., Frenkiel, T. A., Nietlispach, D., and Pastore, A. (2001) Ca^{2+}-independent binding of an EF-hand domain to a novel motif in the α-actinin-titin complex. *Nat. Struct. Biol.* **8,** 853–857
56. Hoeflich, K. P., and Ikura, M. (2002) Calmodulin in action: diversity in target recognition and activation mechanisms. *Cell* **108,** 739–742
57. Littink, K. W., van Genderen, M. M., Collin, R. W., Roosing, S., de Brouwer, A. P., Riemslag, F. C., Venselaar, H., Thiadens, A. A., Hoyng, C. B., Rohrschneider, K., den Hollander, A. I., Cremers, F. P., and van den Born, L. I. (2009) A novel homozygous nonsense mutation in CABP4 causes congenital cone-rod synaptic disorder. *Invest. Ophthalmol. Vis. Sci.* **50,** 2344–2350